



RESEARCH ARTICLE

# Artificial neural network-based control of powered knee exoskeletons for lifting tasks: design and experimental validation

Asif Arefeen  and Yujiang Xiang 

School of Mechanical and Aerospace Engineering, Oklahoma State University, Stillwater, OK, USA

**Corresponding author:** Yujiang Xiang; Email: [yujiang.xiang@okstate.edu](mailto:yujiang.xiang@okstate.edu)

**Received:** 25 July 2023; **Revised:** 9 June 2024; **Accepted:** 6 August 2024; **First published online:** 18 September 2024

**Keywords:** wearable robots; motion planning; artificial neural network; general regression neural network; gradient-based optimization; lifting

## Abstract

This study introduces a hybrid model that utilizes a model-based optimization method to generate training data and an artificial neural network (ANN)-based learning method to offer real-time exoskeleton support in lifting activities. For the model-based optimization method, the torque of the knee exoskeleton and the optimal lifting motion are predicted utilizing a two-dimensional (2D) human–exoskeleton model. The control points for exoskeleton motor current profiles and human joint angle profiles from cubic B-spline interpolation represent the design variables. Minimizing the square of the normalized human joint torque is considered as the cost function. Subsequently, the lifting optimization problem is tackled using a sequential quadratic programming (SQP) algorithm in sparse nonlinear optimizer (SNOPT). For the learning-based approach, the learning-based control model is trained using the general regression neural network (GRNN). The anthropometric parameters of the human subjects and lifting boundary postures are used as input parameters, while the control points for exoskeleton torque are treated as output parameters. Once trained, the learning-based control model can provide exoskeleton assistive torque in real time for lifting tasks. Two test subjects' joint angles and ground reaction forces (GRFs) comparisons are presented between the experimental and simulation results. Furthermore, the utilization of exoskeletons significantly reduces activations of the four knee extensor and flexor muscles compared to lifting without the exoskeletons for both subjects. Overall, the learning-based control method can generate assistive torque profiles in real time and faster than the model-based optimal control approach.

## 1. Introduction

Exoskeletons have the ability to aid humans in physically demanding and injury-prone activities, such as lifting loads while squatting. This aid holds the capability to diminish physical requirements, mitigate related injuries, and potentially alleviate fatigue while maintaining proper postures. Furthermore, it has the capacity to diminish human metabolic energy expenditure and aid in the recovery of abilities lost as a result of strokes and spinal cord injuries [1, 2]. Despite their immense potential, the control of powered exoskeletons remains a persistent challenge.

A significant amount of work has been accomplished by developing lower limb powered exoskeletons over the past several years with the goal of aiding human movement [2, 3]. Researchers have explored diverse optimization-driven dynamic modeling methods to simulate the interaction among individuals utilizing exoskeletons [4–10]. However, there have been limited studies in the literature on the development of exoskeletons for squat and stoop lifting assistance [10–19]. Some researchers have focused solely on developing knee joint exoskeletons to minimize the metabolic cost and reduce muscle fatigue and muscle activity associated with squat lifting [18–22]. Additionally, multiple knee exoskeletons were

developed to aid in tasks involving movement akin to squat lifting, like getting up and sitting down [23, 24].

In the latest research [25–27], notable progress has been observed in the advancement of motorized knee and lower limb exoskeletons, specifically regarding their design and actuation. In addition, learning-based control strategies are getting popular among researchers [28–34], all of which contribute to the efficacy of these devices in assisting with squat lifting, walking, and rehabilitation. Luo et al. [29] presented a new approach to controlling a lower limb exoskeleton using deep reinforcement learning. This method yields a universal controller devoid of any control parameter adjustment. Li et al. [33] presented an overview of cutting-edge control approaches for exoskeletons in lower limb rehabilitation and addressed the current approach to challenges. On the other hand, Masengo et al. [34] discussed the recent development of lower limb exoskeletons, their control approaches, various applications, and problems associated with control systems. Luo et al. [35] presented a novel, deep neural network, reinforcement learning-based robust controller for a lower limb rehabilitation exoskeleton based on a decoupled offline human–exoskeleton simulation training with three independent networks, which can provide reliable walking assistance against various and uncertain human–exoskeleton interaction forces.

This work is the extension of our previous work [10]. Arefeen and Xiang [10] presented an optimal control approach for knee exoskeletons which uses single-case optimization. In this study, we propose a hybrid training model that utilizes a model-based optimization method to generate training data and an artificial neural network (ANN)-based learning method to offer real-time exoskeleton support in lifting activities. For the model-based optimization method, an inverse dynamics optimization formulation is considered to predict the optimal lifting motion and assistive torque. Then, the lifting optimization problem is tackled using a sequential quadratic programming (SQP) algorithm in sparse nonlinear optimizer (SNOPT) [36]. The general regression neural network (GRNN) is used to train the learning-based control model. Once trained, the learning-based control model can provide exoskeleton assistive torque in real time for lifting tasks for any subject in the same age group based on the subject's anthropometric parameters and lifting boundary postures. Two test subjects' joint angles and GRFs comparisons are presented between the experimental (learning-based control) and simulation optimization results. The approach presented in this study provides some unique benefits: (1) this learning-based control approach is faster than the model-based optimal control approach [10] and is computationally efficient. The trained network does not need to compute the optimization problem. (2) The proposed model can be applied to any subject in the same age group with a minimum number of network input parameters.

The structure of the contents is as follows: Section 2 provides a comprehensive explanation of the subject-specific coupled human–exoskeleton model and the equations of motion (EOM). The formulation of the optimization is presented in Section 3. Section 4 thoroughly discusses the experimental procedure and learning-based control approach for the knee exoskeleton. Section 5 provides an analysis of the findings from simulations and experiments. Lastly, Section 6 contains the discussion and concluding remarks.

## 2. Methods

### 2.1. Subject specific coupled human–exoskeleton model

This work focuses on the utilization of a 2D human skeletal model [37], depicted in Figure 1(a). The sagittal plane serves as the axis of symmetry for the model and comprises a total of  $n = 10$  degrees of freedom (DOFs), with three global DOFs. For the experiment, Figure 1(b) demonstrates the attachment of two 1-DOF exoskeletons to the knee joints [10]. To simulate the system, the mass and inertia characteristics of the exoskeleton are taken into account through mathematical analysis. The construction of the human model employs the Denavit–Hartenberg (DH) method [38]. Every DOF relates to the rotation or translation between two parts of the body connected by either a rotating or sliding connection. The degree of freedom for both rotational and translational joints is measured along the local  $z$ -direction. In the global  $Y$ - $Z$  plane, all local rotation joints ( $z_3 \sim z_{10}$ ) rotate in a clockwise direction. The Xsens motion

**Table 1.** DH parameters for the 2D skeletal model.

DOF	$\theta$	$d$	$a$	$\alpha$	Branch
1	$\pi$	0	0	$\pi/2$	Global branch
2	$\pi/2$	$L_4+L_5$	0	$-\pi/2$	
3	0	0	0	0	
4	$-\pi/2$	0	$L_1$	0	Upper body branch
5	$\pi$	0	$L_2$	0	
6	0	0	$L_3$	0	
7	$\pi/2$	0	$L_4$	0	Lower body branch
8	0	0	$L_5$	0	
9	$-\pi/2$	0	$L_6$	0	
10	0	0	$L_7$	0	

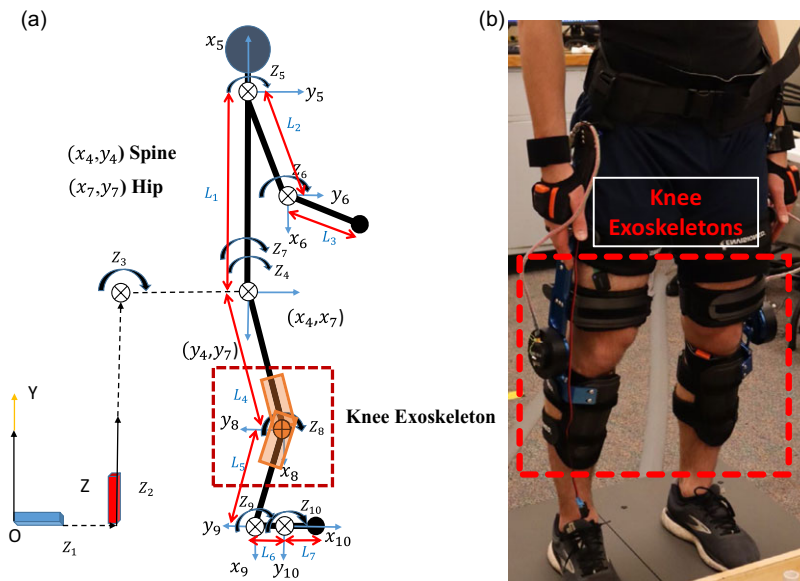


**Figure 1.** (a) The human-exoskeleton model (2D) and (b) Knee exoskeletons.

capture system provides the subject's body measurement data [10]. The human model's DH parameters are shown in Table 1, with  $L_1$  to  $L_7$  representing the lengths of the respective joint links in the human body. These joint link lengths are different and unique for different humans. As a result, our 2D model can be scaled for different individuals.

The human model's kinematics and dynamics are through recursive kinematics and Lagrangian dynamics [39, 40]. In addition, this study includes the modeling of the electromechanical dynamics of DC motors used in exoskeletons [10]. (See Appendix: Kinematics and dynamics)

### 3. Lifting optimization Formulation

#### 3.1. Design variables

A cubic B-splines interpolation is employed to discretize  $I(t)$  and  $q(t)$  [41]. The design variables ( $\mathbf{x}$ ) consist of the control points  $\mathbf{P}_{human}$  for human joint angle and the control points  $\mathbf{P}_{current}$  for exoskeleton current. Therefore, the design variables are  $\mathbf{x} = [\mathbf{P}_{human}^T \mathbf{P}_{current}^T]^T$ .

### 3.2. Objective function

In this study, the sum of squared normalized human joint torques is treated as the cost function [10, 40–42]:

$$\min_{\mathbf{x}} J_1(\mathbf{x}) = \sum_{i=3}^n \int_0^T \left[ \frac{\tau_{hi}(\mathbf{x})}{(\tau_i^U - \tau_i^L)} \right]^2 dt \quad (1)$$

where  $T$  is the designated overall duration for the lifting operation, and  $\tau_i^U$  and  $\tau_i^L$  stand for the upper and lower boundaries of torque pertaining to the human  $i^{th}$  joint.

### 3.3. Constraints

Time-dependent constraints are calculated sequentially at each time point in the optimization process. On the other hand, the optimization process evaluates time-independent constraints at specific times rather than throughout the entire motion. Table 2 presents the time-dependent and time-independent constraints [10].

## 4. Control approach and experimental procedure

### 4.1. Hybrid training model

In this study, we have created a hybrid training model that includes data from experiments and model simulations to generate training data for the learning-based control model. The anthropometric parameters of the human subjects from the experiment are used as input parameters for the model-based method, as discussed in section 2.1. We have collected data from three subjects, as shown in Table 3. The input parameters of the lifting task include the subject's weight, the subject's height (head length, neck length, spine length, and hip to foot length), and initial, middle, and final postures (spine, shoulder, elbow, hip, knee, and ankle joints). For the learning-based model, the input training cases are created as various combinations of values from Table 3 [44]. For example, first training case, the subject's weight, subject's height, and initial, middle, and final posture values are set to subject-1. The next training case is formulated by keeping the subject's weight, subject's height, and initial and middle posture values at subject-1 and moving the subject's final posture values to subject-2. For the third training case, the subject's final posture values are set to subject-3 by keeping the subject's weight, subject's height, and initial and middle posture values at subject-1. Using this process for the three subjects, we have created 243 training cases for input parameters: subject's weight, subject's height (group of link lengths), initial postures (group of joint angles), middle postures (group of joint angles), and final postures (group of joint angles). It is possible to create more training cases by increasing the total number of subjects and the number of input parameters for each subject. In the model-based method, we have used inverse dynamics optimization to find the optimal lifting motion and assistive exoskeleton torque. Finally, we have employed the least square optimization to transfer the optimal exoskeleton torque control points from the time domain to the joint angle domain, which are used as output parameters for the training, as presented in Figure 2 [10]. On a computer with an Intel® Core™ i7 2.11 GHz CPU and 16 GB RAM, the average simulation time for each training case is 0.54 s CPU time.

For each training case and lifting task, optimization-1 finds  $(\tau_{exo}^*)_i(t)$  (optimal exoskeleton torque) and  $(\theta_k^*)_i(t)$  (optimal knee angle) for the  $i^{th}$  optimization, as illustrated in Figure 2 [10]. In order to express  $(\tau_{exo}^*)_i(\theta_e)$ , B-spline interpolation is utilized, where  $\theta_e$  is the knee exoskeleton's encoder angle. Using the least square optimization, optimization-2 finds  $(\mathbf{P}_{\tau_{exo}})_i$  (exoskeleton torque control points) for  $(\tau_{exo}^*)_i(\theta_e)$  (exoskeleton torque as a function of encoder angle) [10].

### 4.2. Learning-based control method

We use an ANN, specifically a GRNN to train the hybrid model data from section 4.1 [44], as shown in Figure 3. The GRNN represents a form of a radial basis network (RBN) that offers a global solution while

Table 2. Constraints.

Time dependent	Time independent
<p>1. Joint angle limits</p> $\mathbf{q}^L \leq \mathbf{q}(\mathbf{x}, t) \leq \mathbf{q}^U$ <p>where <math>\mathbf{q}^L</math> and <math>\mathbf{q}^U</math> are the lower and upper human joint limits [10, 43].</p> <p>2. Joint torque limits</p> $\boldsymbol{\tau}^L \leq \boldsymbol{\tau}(\mathbf{x}, t) \leq \boldsymbol{\tau}^U$ <p>where <math>\boldsymbol{\tau}^L</math> and <math>\boldsymbol{\tau}^U</math> are the lower and upper human joint torque limits [10, 43].</p> <p>3. Feet contacting position</p> $p_{feet}(\mathbf{x}, t) = p_{feet}^s$ <p>where <math>p_{feet}^s</math> is the specified feet contact position on level ground.</p> <p>4. Box forward position</p> $Z_{wrist}(\mathbf{x}, t) - Z_{pelvis}(\mathbf{x}, t) \geq 0$ <p>where <math>Z_{wrist}</math> and <math>Z_{pelvis}</math> are the global Z coordinates of the human wrist and pelvis points [39].</p> <p>5. Collision avoidance</p> $d_{human}(\mathbf{x}, t) \geq r_{human}$ <p>where <math>d_{human}</math> is the calculated distance between the hand and the circle center on the body segment representing the body thickness, and <math>r_{human}</math> is the radius of the circle filled on human limbs [10].</p> <p>6. Stability condition</p> $p_{human\_ZMP}(\mathbf{x}, t) \in \text{FSR}$ <p>where zero moment point (ZMP) position is inside the foot support region (FSR) for human [39].</p> <p>7. Exoskeleton torque boundaries</p> $\boldsymbol{\tau}_{exo}^L \leq \boldsymbol{\tau}_{exo}(\mathbf{x}, t) \leq \boldsymbol{\tau}_{exo}^U$ <p>where <math>\boldsymbol{\tau}_{exo}^L</math> is lower torque boundary and <math>\boldsymbol{\tau}_{exo}^U</math> is the upper boundary for the exoskeleton [10].</p>	<p>1. Initial and final hand positions</p> $p_{humanhand}(\mathbf{x}, t) = p_{humanhand}^s(t); t = 0, T$ <p>2. Initial and final static conditions</p> $\dot{\mathbf{q}}_{human}(\mathbf{x}, t) = \mathbf{0}; t = 0, T$ <p>3. Initial, mid-time, and final joint angles for the human joints</p> $ q_{i_{human}}(\mathbf{x}, t) - q_{i_{human}}^E(t)  \leq \varepsilon; t = 0, \frac{T}{2}, T$ <p>where <math>\varepsilon = 0.2</math> and <math>q_{i_{human}}^E</math> is the experimental joint angle for the human joints.</p>

optimizing the network parameter values during training [44]. The architecture of the GRNN model, implemented using the MATLAB toolbox, consists of two layers: the RBF hidden layer and the linear output layer [45]. Once GRNN has been trained, the trained model can provide the exoskeleton torque control points ( $\mathbf{P}_{\tau_{exo}}$ ) for any subject's (same age group) input parameters, as illustrated in Figure 4. These exoskeleton torque control points are considered for the calculations of the exoskeleton torque ( $\tau_{exo}(\theta_e)$ ) in real time by using the B-spline interpolation during the lifting process (Figure 4). It is important to note that in order to provide support, the encoder angle has to fall within the stated initial and final boundary restrictions. If not, a lower predetermined constant assistance of  $\tau_{exo} = 2.1$  Nm is offered [10].

Based on Table 4 input parameters, a comparison between the exoskeleton torque profile obtained from optimization (section 4.1) and learning-based control (section 4.2) is illustrated in Figure 5. Additionally, a statistical analysis of  $R^2$  values of the exoskeleton torque are calculated between optimal and GRNN results, as presented in Figure 6.

**Table 3.** Input parameter for three subjects.

Input parameter	Subject-1	Subject-2	Subject-3
Subject weight (kg)	81.36	76.37	82.27
Subject height (m)	Head length	0.157	0.139
	Neck length	0.129	0.118
	Spine length	0.635	0.568
	Hip to football	0.979	0.875
	Spine angle	39.746	26.525
Initial postures (degrees)	Shoulder angle	−91.472	−63.779
	Elbow angle	−27.876	−31.436
	Hip angle	−130.698	−118.072
	Knee angle	106.479	124.04
	Ankle angle	−8.670	−8.670
Middle postures (degrees)	Spine angle	14.998	22.662
	Shoulder angle	−65.915	−48.804
	Elbow angle	−36.33	−37.748
	Hip angle	−40.99	−54.070
	Knee angle	30.891	36.768
Final postures (degrees)	Ankle angle	−4.411	−9.411
	Spine angle	5.627	4.495
	Shoulder angle	−23.931	−21.84
	Elbow angle	−78.751	−38.514
	Hip angle	−0.433	7.676
	Knee angle	7.911	5.075
	Ankle angle	−4.481	−5.714

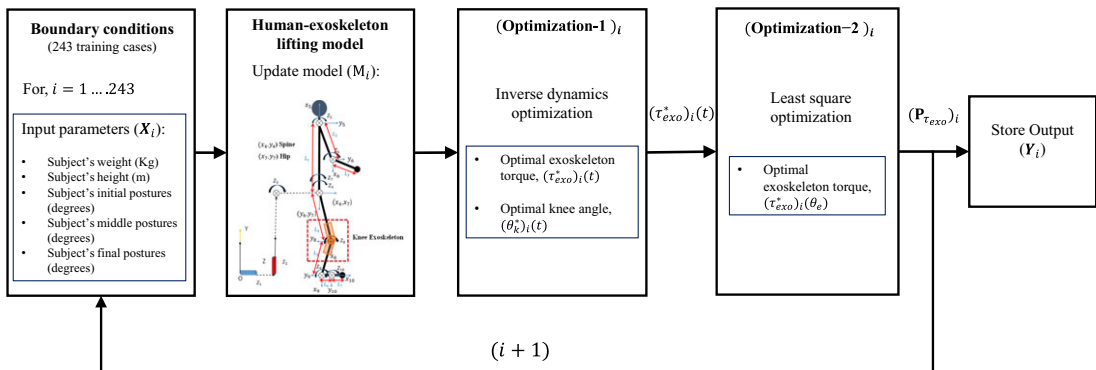


**Figure 2.** The hybrid model to generate training data for the learning-based control model.  $(P_{\tau_{exo}})_i$  is the optimal exoskeleton torque control point  $(7 \times 1)$  for the  $i^{th}$  optimization.  $X_i$  and  $Y_i$  are the input  $(23 \times 1)$  and output training data  $(7 \times 1)$  for the ANN, respectively.

### 4.3. Experimental procedure

The learning-based control lifting experiment was performed at Oklahoma State University's Biodynamics Optimization Lab, following approval from the Institutional Review Board (IRB). For this study, we considered two groups of subjects: (1) training GRNN group and (2) test subjects group for validation. All subjects were free of any prior injuries, and they each signed a written consent form before the experiment. For training the GRNN group, we recruited three healthy subjects with an age range of 22–30 years. The subjects' anthropometric measurements were taken, as presented in Table 3.

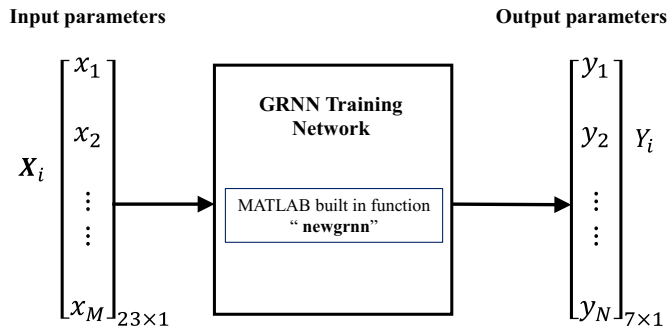


**Figure 3.** The GRNN training for learning-based control.

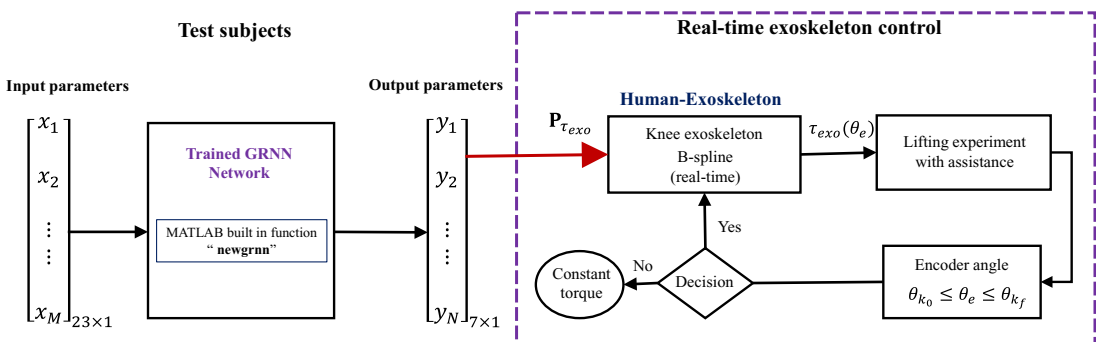


**Figure 4.** Learning-based exoskeleton control algorithm for any subject in the same age group.

For 3D kinematic information, the Xsens motion capture system was employed at a frequency of 60 Hz, while the entire body sensors procedure was taken into account, as shown in Figure 7.

For the test subjects' group, we selected three healthy subjects within an age range of 21–30 years. The participants visited the lab twice. Anthropometric measurements of the individuals were acquired on the initial visit, and a similar protocol to that of the first group was followed, as presented in Table 4. During the second visit, the experiment was conducted in two stages: (a) without exoskeletons and test subject-1 and test subject (b) with exoskeletons, as illustrated in Figure 8. The subject's maximum voluntary contractions (MVCs) were initially recorded from the subject's right leg's vastus medialis, vastus lateralis, rectus femoris, and biceps femoris muscles at 2000Hz [10]. Each muscle underwent three trials during the MVC testing [46, 47], with each trial separated by a 30 s rest period. During the lifting tasks without an exoskeleton, the subject lifted an 11 kg box while standing on two Bertec force plates. The participant utilized the squat lifting strategy for this task. Xsens's MVN Analyze Pro software recorded the lifting motion, while OptiTrack Motive 3.0 software recorded the ground reaction forces (GRFs) at 1000 Hz. Additionally, the raw EMG data was recorded using EMGworks Acquisition. With a 3-minute pause in between each lifting session, the task was performed three times. All the data were processed in MVN Analyze, Motive 3.0 and MATLAB [10]. For the two force plates, the mean value was calculated for each trial's processed GRFs. In the end, the three experimental attempt averages were evaluated to the predicted results.

In this study, the powered wearable knee exoskeletons created by Picasso Intelligence, LLC [10] were employed for the lifting task with exoskeletons. The suggested learning-based control approach was implemented. Subsequently, the participant was instructed to don the exoskeleton and repeat the lifting task, as shown in Figure 8. The subject's 3D kinematic data, EMG raw data, and GRFs were recorded, just like during the first visit. In addition, with a 3-minute pause in between each lifting session, the task was performed three times.

*Table 4.* Input parameter for test subjects.

Input parameter		Test subject-1	Test subject-2	Test subject-3
Subject height (m)	Subject weight (kg)	88.97	68.75	77.91
	Head length	0.1516	0.1379	0.1485
	Neck length	0.1248	0.1180	0.1233
	Spine length	0.6108	0.5655	0.6011
	Hip to football	0.9328	0.8786	0.9221
Initial postures (degrees)	Spine angle	17.962	18.311	34.562
	Shoulder angle	−81.601	−90.627	−89.276
	Elbow angle	−3.989	−15.984	−19.933
	Hip angle	−117.302	−119.142	−130.013
	Knee angle	120.348	126.354	116.613
Middle postures (degrees)	Ankle angle	−6.512	−9.461	−6.369
	Spine angle	13.035	5.428	17.341
	Shoulder angle	−70.959	−83.438	−87.647
	Elbow angle	−12.935	−20.383	−20.219
	Hip angle	−51.728	−29.378	−48.682
Final postures (degrees)	Knee angle	51.784	21.884	36.309
	Ankle angle	−6.458	−10.120	−4.076
	Spine angle	8.808	21.548	8.687
	Shoulder angle	−23.016	−82.547	−82.284
	Elbow angle	−47.835	−20.684	−25.926
Final postures (degrees)	Hip angle	15.256	19.017	6.050
	Knee angle	5.943	1.546	2.987
	Ankle angle	−8.032	−10.027	−0.880

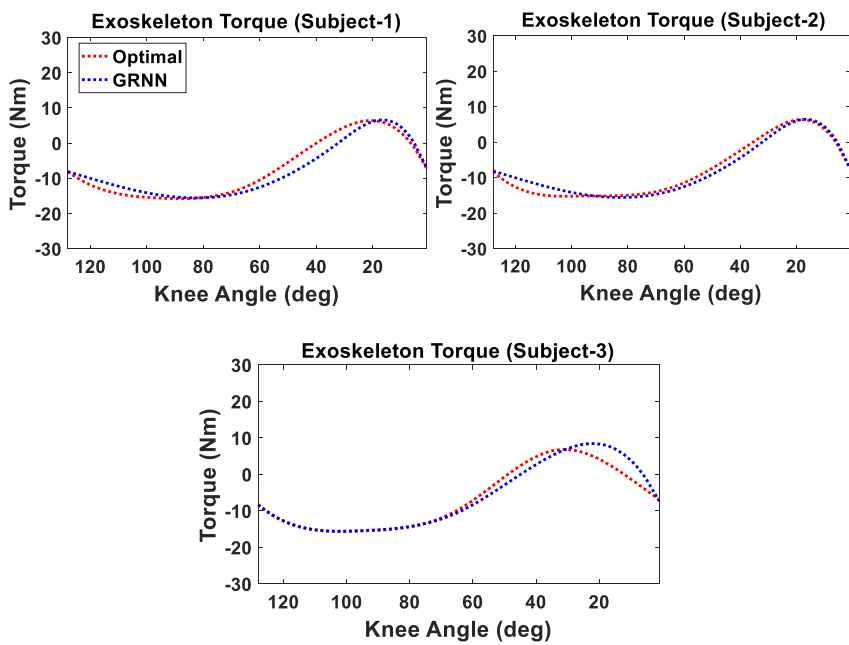


**Figure 5.** Comparison between optimal and learning (GRNN) control-based exoskeleton torque profiles with maximum 16 Nm torque on each knee.

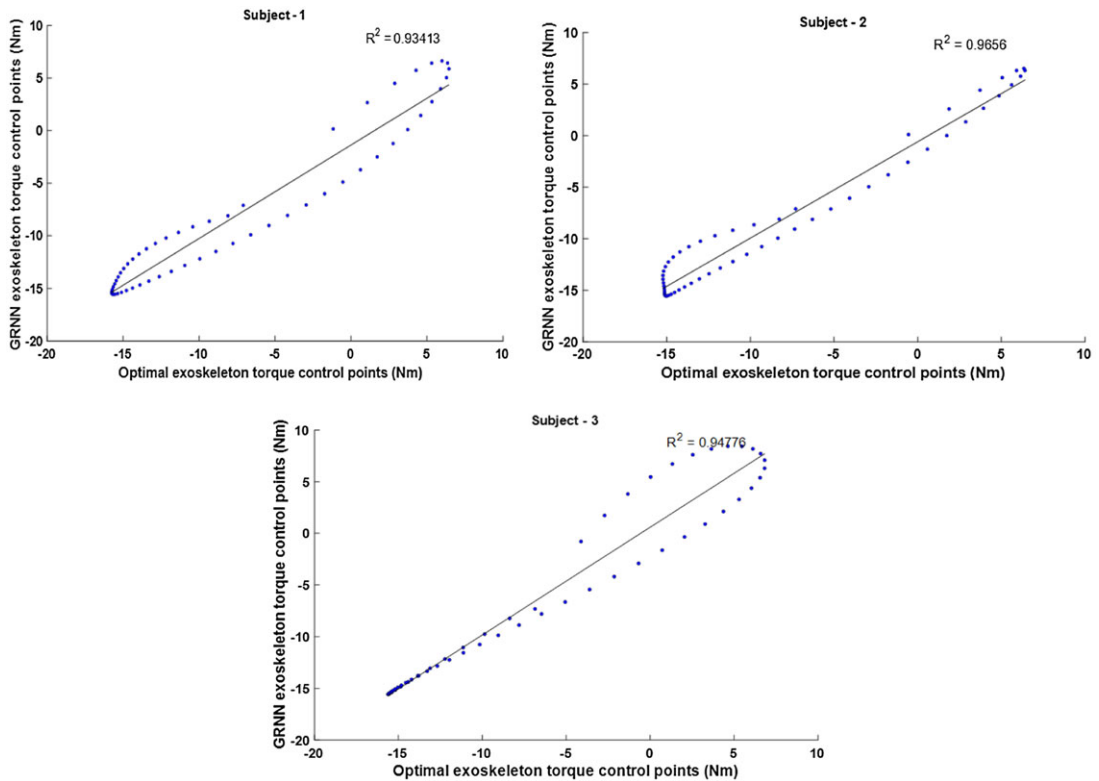


**Figure 6.** Statistical analysis (between optimal and GRNN) for the exoskeleton torque control in test subjects 1, 2, and 3.



**Figure 7.** Training GRNN group (three subjects).

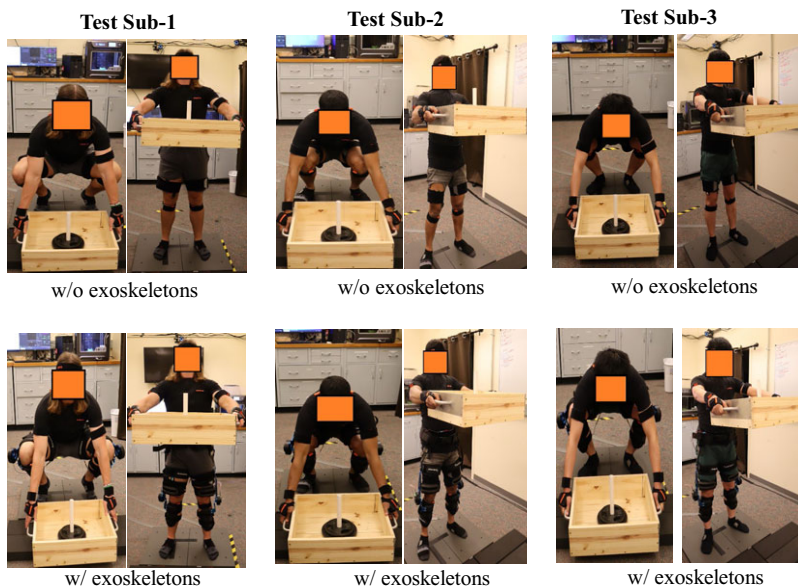


**Figure 8.** Test subjects for validation (three subjects).

## 5. Results

In SNOPT, a SQP approach is adopted to address the lifting problem [36]. For the optimization, the starting assumption is  $\mathbf{x} = [\mathbf{P}_{human}^T \ \mathbf{P}_{current}^T]^T = [\mathbf{0}]$ . For the lifting optimization without exoskeleton, we have considered five control points ( $nctrl = 5$ ) for each human joint angle profile in the cubic B-spline interpolation. The optimal solution for test subject simulation is obtained in 0.24 s CPU time.

For the optimization of lifting with the exoskeleton, there are two processes: (1) inverse dynamics optimization and (2) least square optimization, as illustrated in Figure 2. The DC motor's electrical and mechanical characteristics are discussed in ref. [10]. The optimization takes into account the exoskeleton torque boundaries between  $-16$  Nm and  $16$  Nm. For the least square optimization, we have considered seven control points ( $nctrl\_exo = 7$ ) for B-spline interpolation at each exoskeleton joint. Having more control points increases the accuracy of continuous mapping from the time domain to the angle domain. The optimal solution is obtained in 0.39 s CPU time. A computer equipped with an Intel® Core™ i7 2.11 GHz CPU and 16 GB RAM is utilized for the optimization process. The input data for the box-lifting task can be found in ref. [10].

### 5.1. Simulation and experimental comparison (without the exoskeleton)

Figures 9 and 10 demonstrate a comparison between the experimental and simulated angles of various joints (spine, shoulder, elbow, hip, knee, and ankle) in the human body for test subjects 1 and 2. Similarly, Figures 11 and 12 present a comparison of the horizontal and vertical GRFs for the same subjects, both in experimental and simulation scenarios.

### 5.2. Simulation and experimental comparison (with the exoskeleton)

The analysis of various joint angles (spine, shoulder, elbow, hip, knee, and ankle) in the human body, based on experimental and simulation data for test subjects 1 and 2, is displayed in Figures 13 and 14. The comparison of the horizontal and vertical GRFs for participants 1 and 2 between experiments and simulations is shown in Figures 15 and 16.

( Test Subject-1 )

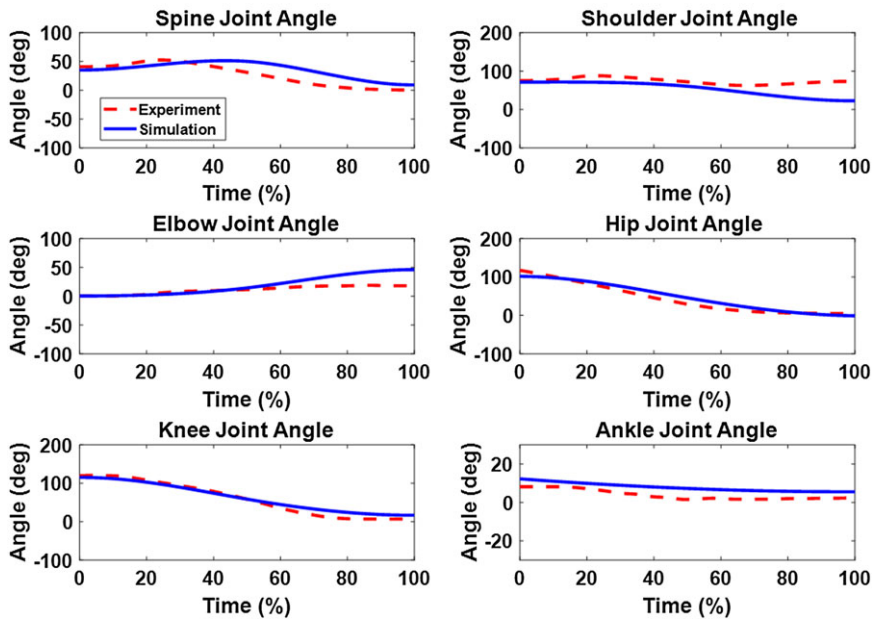


Figure 9. Joint angle profiles comparison without exoskeletons (test subject-1).

( Test Subject-2 )

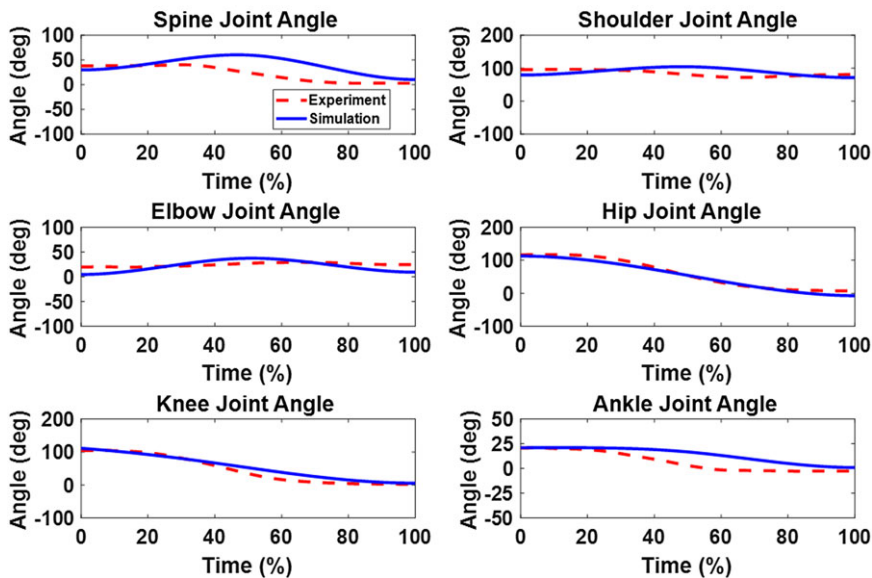
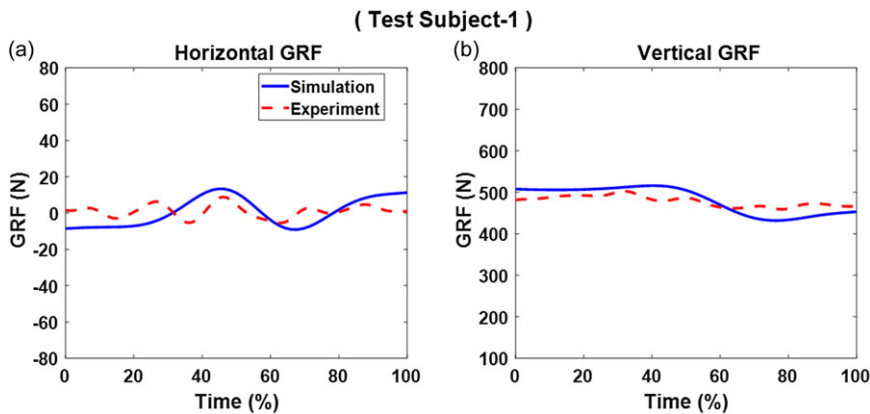


Figure 10. Joint angle profiles comparison without exoskeletons (test subject-2).

### 5.3. Muscle activation comparison

The muscle activation comparisons for test subjects 1, 2, and 3 from the experiments, with and without exoskeletons, are shown in Figures 17, 18 and 19.



**Figure 11.** GRFs comparison without exoskeletons (test subject-1).

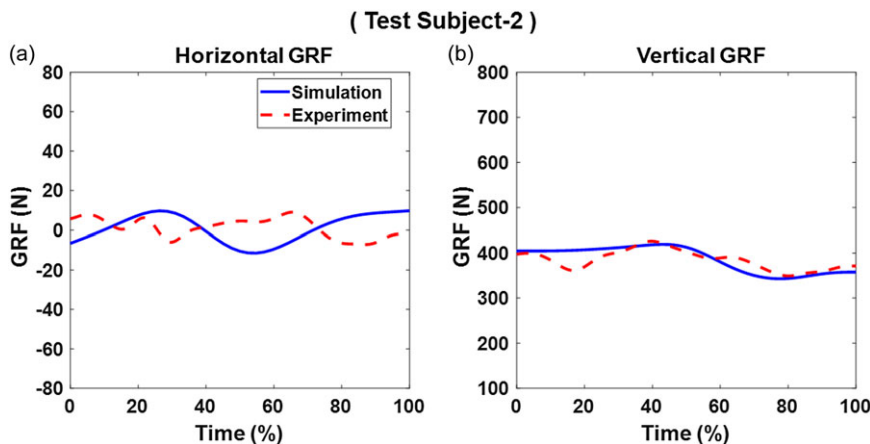


**Figure 12.** GRFs comparison without exoskeletons (test subject-2).

## 6. Discussion

The predicted joint angles (spine, shoulder, elbow, hip, knee, and ankle) matched well with the experimental results in Figures 9 and 10 for test subjects 1 and 2. The predicted GRFs trends closely follow the experiment GRFs trends, as shown in Figures 11 and 12. However, the predicted vertical GRF (test subject-1) values are within 0.85% of the experimental GRF, with peak value differences of 2.60%. As for test subject-2, the predicted vertical GRF values are within 0.68% of the experimental GRF, with peak value differences of 1.63%.

For the lifting with exoskeletons, the joint angle comparisons (Figures 13 and 14) show similar trends and magnitudes in the predicted joint angle profiles (optimization) for both subjects, as compared to the experimental data (learning-based control). We also see that upper body joints exhibit greater differences than lower body joints. In Figures 15 and 16, horizontal GRFs exhibit similar trends and magnitude for test subjects 1 and 2. The predicted vertical GRFs also match the experimental GRFs by 2.78% and 4.79%, respectively. The peak value differences are 0.05% and 3.57% for test subject-1 and test subject-2, respectively.

We consider four muscles from the lower extremity for muscle activation comparison: knee extensors (rectus femoris, vastus medialis, and vastus lateralis) and knee flexors (biceps femoris), as shown in Figures 17, 18, and 19. With and without exoskeletons, the patterns of muscle activations show resemblance in both scenarios. Nonetheless, for both test subjects, the exoskeletons considerably lessen these

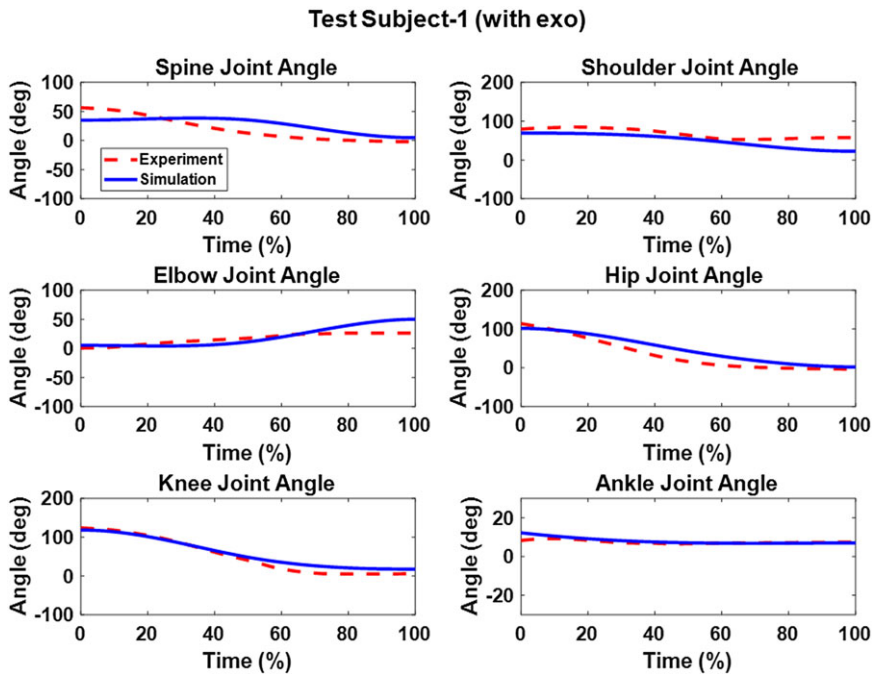


**Figure 13.** Joint angle profiles comparison with exoskeletons (test subject-1).

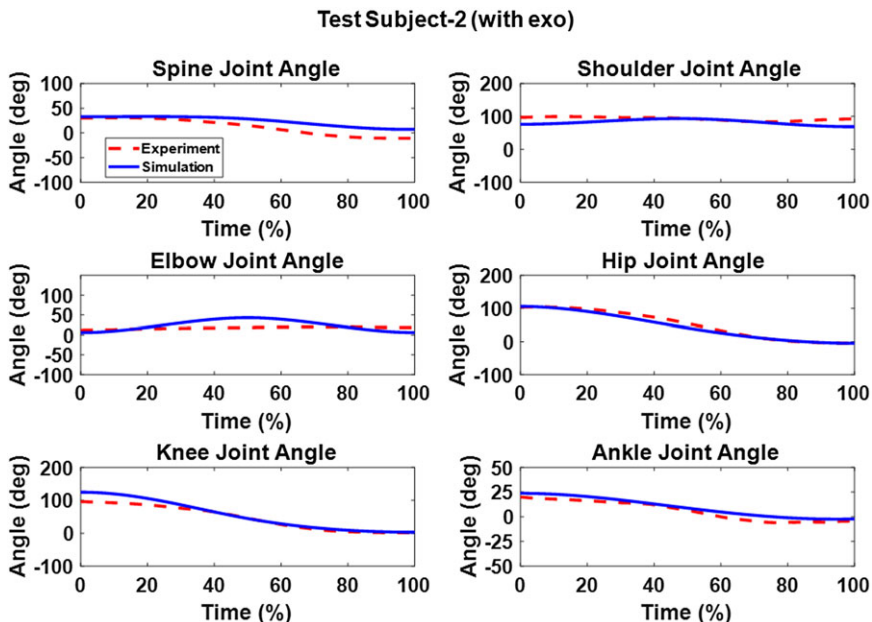


**Figure 14.** Joint angle profiles comparison with exoskeletons (test subject-2).

muscle activations. For test subject-1, the peak values are seen to be decreased by 22.46%, 26.46%, 4.74%, and 7.72%, respectively, of the vastus medialis, vastus lateralis, biceps femoris, and rectus femoris muscles. Additionally, the mean values of the same muscle group with exoskeleton support are 0.117, 0.136, 0.038, and 0.146, respectively. The mean values for the same muscle group in the absence

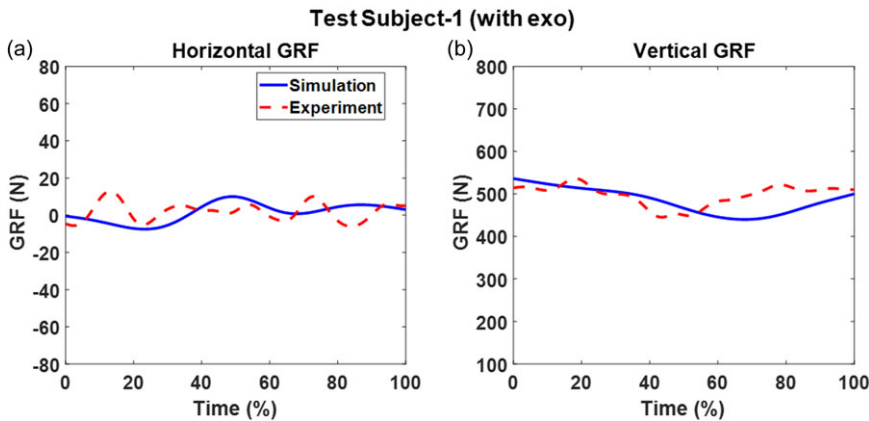


Figure 15. GRFs comparison with exoskeletons (test subject-1).

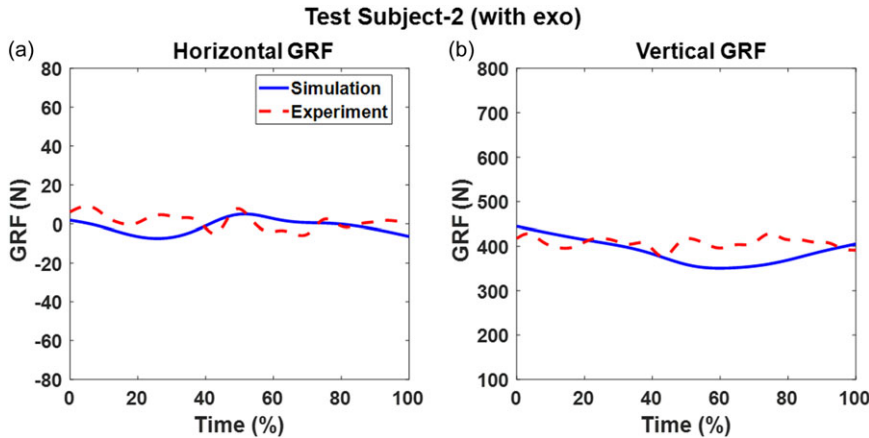
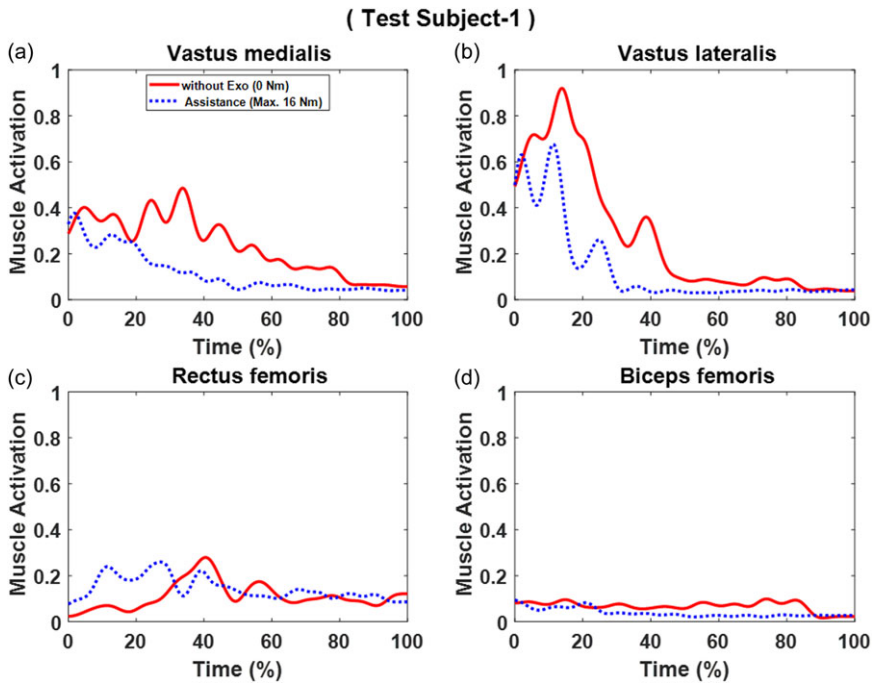


Figure 16. GRFs comparison with exoskeletons (test subject-2).

of exoskeletons are 0.236, 0.276, 0.068, and 0.112, respectively. Thus, when comparing the mean values of the four muscles activation with and without exoskeleton, there are certain percentage decreases observed for vastus medialis, vastus lateralis, and biceps femoris muscles activation. Specifically, the percentage decreases for these muscles are 50.42%, 50.77%, and 43.62% for the test subject-1. Notably, while the peak value for rectus femoris muscle activation decreases, the mean value percentage increases by 30.25% for test subject-1.

Test subject-2 exhibits reductions of 46.34%, 47.22%, 49.05%, and 7.46% in peak values for the vastus medialis, vastus lateralis, biceps femoris, and rectus femoris, respectively. Additionally, the mean muscle activation values for vastus medialis, vastus lateralis, biceps femoris, and rectus femoris with exoskeleton assistance are 0.094, 0.201, 0.154, and 0.248, respectively. Without the exoskeleton, these values have changed to 0.124, 0.277, 0.219, and 0.328 for the same muscles. Consequently, when comparing the mean values of the four muscles with and without the exoskeleton, there are percentage decreases of 24.60%, 27.66%, 29.89%, and 24.60%, respectively. For test subject-3, the peak values of the vastus medialis, vastus lateralis, biceps femoris, and rectus femoris muscles are decreased by 11.30%, 23.32%, 23.11%, and 28.42%, respectively. Additionally, the mean value percentages are decreased by 22.35%, 11.99%, 35.67%, and 38.16%, respectively.

The effectiveness of single dynamic effort objective function has been proved in the literature for walking [40], running [48], lifting [49], and jumping [50] simulations. Therefore, in this study, we used



**Figure 17.** Test subject-1 muscle activations comparison between with and without exoskeletons.

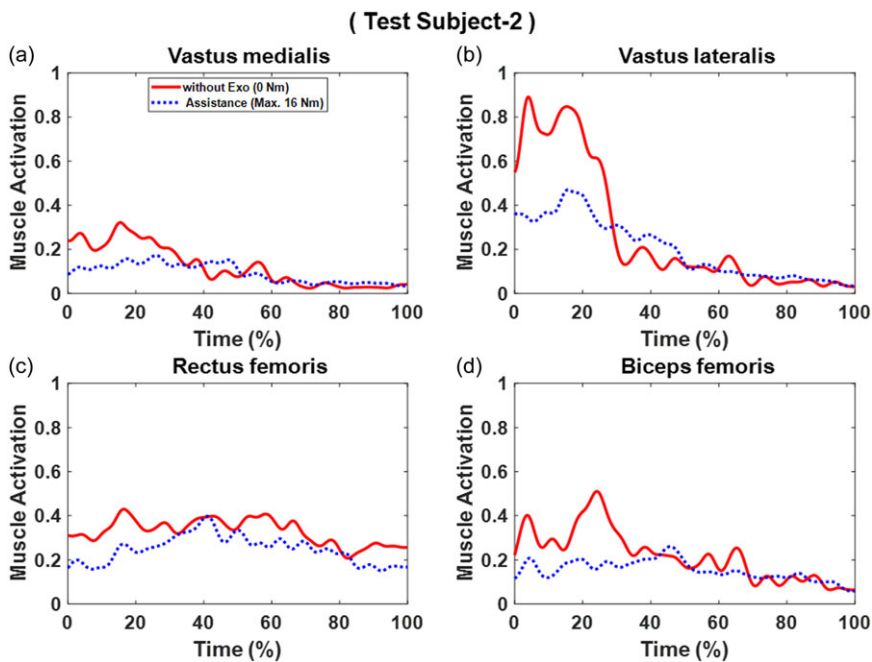


**Figure 18.** Test subject-2 muscle activations comparison between with and without exoskeletons.

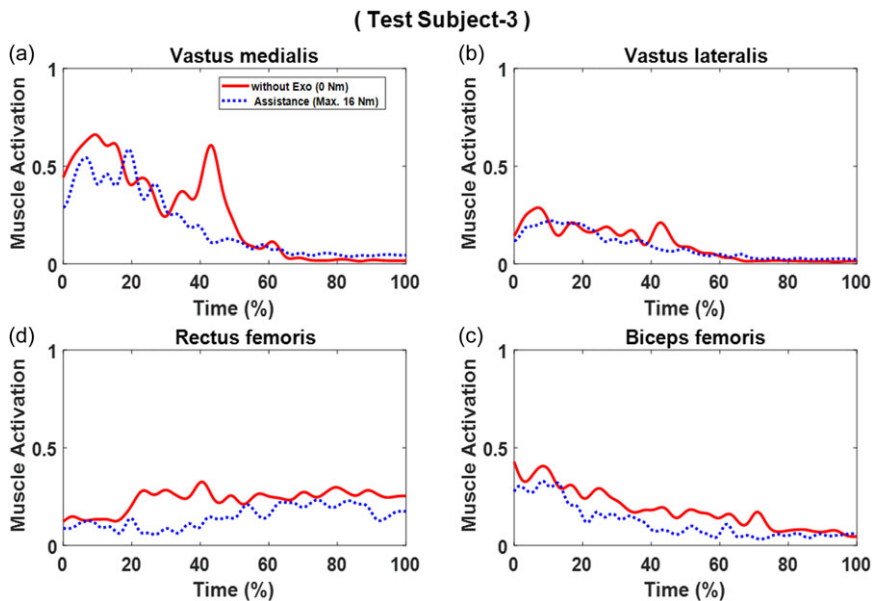


**Figure 19.** Test subject-3 muscle activations comparison between with and without exoskeletons.

the dynamic effort single-objective function. In the literature, many multi-objective (MOO) functions were used for lifting simulation, such as combinations of dynamic effort and stability [41], joint effort and box weight [43], joint effort and initial postures [51], and joint effort and muscle effort [52]. For MOO, it is not an easy task to determine the appropriate weighting coefficients for each objective function. Generally, experimental error analysis is required to decide those coefficients [41]. In addition, in this study, the dynamic effort single-objective function and appropriate constraints optimization formulation generated acceptable regressions, as shown in Figure 6. Therefore, we can use a single objective in this research. Exploring other MOO will be future research.

Three subjects are a good combinations of learning set for GRNN learning method. This has been proved for human motion prediction in the literature [44]. In addition, we demonstrated statistically that the regression results are reliable (Figure 6). Furthermore, we tried four training subjects dataset, and there was no obvious improvement in terms of regression accuracy.

In Figure 5, we have compared the optimization method with the GRNN learning approach and the results matched very well. The optimization method was used in the literature for predicting exoskeleton assistive torques [53–56]. Our learning method has comparable accuracy. Other learning approaches require a different amount of training data, and it is not applicable in this research.

## 7. Conclusions

In this study, we propose a hybrid model that utilizes a model-based optimization method to generate training data and an ANN-based learning method to offer real-time exoskeleton support in lifting activities. For the model-based optimization method, an inverse dynamics optimization formulation is used to predict the optimal lifting motion and assistive torque. The GRNN is used to train the learning-based control model based on the training input and output data from model-based optimization method. Once trained, the learning-based control model can provide exoskeleton assistive torque in real time for lifting tasks for any subject in the same age group, based on the subject's anthropometric parameters and lifting boundary postures. We present joint angles and GRFs comparisons between the experimental and simulation results for two random test subjects. The simulation results match well with the experimental data.

Furthermore, exoskeletons significantly reduce knee extensor and flexor muscle activations compared to lifting without the exoskeletons for both subjects. Overall, the learning-based control method can generate assistive torque profiles in real time and faster than the model-based optimal control approach. Consequently, the suggested learning-oriented control system of the powered knee exoskeleton can help alleviate dynamic human exertion and reduce the occurrence of injuries while lifting objects. One constraint of this study is that we solely focus on the squat lifting approach. In forthcoming research, we intend to explore the semi-squat and stoop lifting methods as well. Furthermore, we aim to assess our model using various learning-based methodologies to facilitate comparison.

**Acknowledgments.** The authors would like to thank the participant for the experimental data collection for this work. This work was partially supported by the National Science Foundation (CBET 2014281).

**Author contribution.** A.A. and Y.X. contributed to the study conception and design. A.A. performed data collection and analysis. A.A. and Y.X. wrote the main manuscript text. Y.X. supervised this work. All authors read and approved the final manuscript.

**Financial support.** This study is supported by Research Jumpstart/Accelerator Grant from Oklahoma State University.

**Competing interests.** The authors declare none.

**Code or data availability.** No.

**Ethical standards.** The authors assert that all procedures contributing to this work comply with the ethical standards of the relevant national and institutional committees on human experimentation and with the Helsinki Declaration of 1975, as revised in 2008.

## References

- [1] X. Tang, X. Wang, X. Ji, Y. Zhou, J. Yang, Y. Wei and W. Zhang, “A wearable lower limb exoskeleton: Reducing the energy cost of human movement,” *Micromachines* **13**(6), 900 (2022).
- [2] D. Terrazas-Rodas, L. Rocca-Huaman, C. Ramírez-Amaya and A. E. Alvarez-Rodriguez, “Lower-Limb Exoskeleton Systems for Rehabilitation and/or Assistance: A Review,” *In: 2022 IEEE International IOT, Electronics and Mechatronics Conference (IEMTRONICS)*, Toronto, ON, Canada (IEEE, 2022) pp. 1–7.
- [3] A. J. Young and D. P. Ferris, “State of the art and future directions for lower limb robotic exoskeletons,” *IEEE Trans Neur Syst Rehabil Eng* **25**(2), 171–182 (2016).
- [4] S. Bai and J. Rasmussen, “Modelling of Physical Human-Robot Interaction for Exoskeleton Designs,” *In: Proc. of Multibody Dynamics 2011, ECCOMAS Thematic Conference*, Brussels, Belgium (2011).
- [5] P. Agarwal, P. H. Kuo, R. R. Neptune and A. D. Deshpande, “A Novel Framework for Virtual Prototyping of Rehabilitation Exoskeletons,” *In: 2013 IEEE 13th International Conference on Rehabilitation Robotics (ICORR)*, Seattle, WA, USA (IEEE, 2013) pp. 1–6.
- [6] K. Cho, Y. Kim, D. Yi, M. Jung and K. Lee, “Analysis and Evaluation of a Combined Human-Exoskeleton Model Under Two Different Constraints Condition,” *In: Proceedings of the International Summit on Human Simulation*, Pete Beach, FL (2012).
- [7] X. Zhou and X. Chen, “Design and evaluation of torque compensation controllers for a lower extremity exoskeleton,” *J Biomech Eng* **143**(1), 011007 (2021).
- [8] A. Arefeen and Y. Xiang, “Modeling and Simulation of a Powered Exoskeleton System to Aid Human-Robot Collaborative Lifting,” *In: Proceedings of the 7th International Digital Human Modeling Symposium (DHM 2022) and Iowa Virtual Human Summit 2022*, Iowa city, USA (2022).
- [9] A. Arefeen and Y. Xiang, “Optimal Control of Spine and Shoulder Powered Exoskeletons for Squat Lifting,” *In: Proceedings of the ASME. 2023 International Design Engineering Technical Conferences and Computers and Information in Engineering Conference*, Boston, Massachusetts (2023). 2023-08-20
- [10] A. Arefeen and Y. Xiang, “Subject specific optimal control of powered knee exoskeleton to assist human lifting tasks under controlled environment,” *Robotica* **41**(9), 2809–2828 (2023).
- [11] W. Wei, S. Zha, Y. Xia, J. Gu and X. Lin, “A hip active assisted exoskeleton that assists the semi-squat lifting,” *Appl Sci* **10**(7), 2424 (2020).
- [12] P. Manns, M. Sreenivasa, M. Millard and K. Mombaur, “Motion optimization and parameter identification for a human and lower back exoskeleton model,” *IEEE Robot Autom Lett* **2**(3), 1564–1570 (2017).

- [13] M. Harant, M. Sreenivasa, M. Millard, N. Šarabon and K. Mombaur, "Parameter Optimization for Passive Spinal Exoskeletons based on Experimental Data and Optimal Control," *In: 2017 IEEE-RAS 17th International Conference on Humanoid Robotics (Humanoids)*, Birmingham, UK (IEEE, 2017) pp. 535–540.
- [14] M. Millard, M. Sreenivasa and K. Mombaur, "Predicting the motions and forces of wearable robotic systems using optimal control," *Front Robot AI* **4**, 41 (2017).
- [15] U. Heo, S. J. Kim and J. Kim, "Backdrivable and fully-portable pneumatic back support exoskeleton for lifting assistance," *IEEE Robot Autom Lett* **5**(2), 2047–2205 (2020).
- [16] A. S. Koopman, S. Toxiri, V. Power, I. Kingma, J. H. van Dieën, J. Ortiz and M. P. de Looze, "The effect of control strategies for an active back-support exoskeleton on spine loading and kinematics during lifting," *J Biomech* **91**, 14–22 (2019).
- [17] X. Yang, T. H. Huang, H. Hu, S. Yu, S. Zhang, X. Zhou and H. Su, "Spine-inspired continuum soft exoskeleton for stoop lifting assistance," *IEEE Robot Autom Lett* **4**(4), 4547–4554 (2019).
- [18] T. Zhang and H. Huang, "A lower-back robotic exoskeleton: Industrial handling augmentation used to provide spinal support," *IEEE Robot Autom Mag* **25**(2), 95–106 (2018).
- [19] F. Sado, H. J. Yap, R. A. R. Ghazilla and N. Ahmad, "Design and control of a wearable lower-body exoskeleton for squatting and walking assistance in manual handling works," *Mechatronics* **63**, 102272 (2019).
- [20] A. Gams, T. Petrič, T. Debevec and J. Babič, "Effects of robotic knee exoskeleton on human energy expenditure," *IEEE Trans Biomed Eng* **60**(6), 1636–1644 (2013).
- [21] Z. Wang, X. Wu, Y. Zhang, C. Chen, S. Liu, Y. Liu, A. Peng and Y. Ma, "A semi-active exoskeleton based on EMGs reduces muscle fatigue when squatting," *Front Neurorobot* **15**, 625479 (2021).
- [22] S. Yu, T. H. Huang, D. Wang, B. Lynn, D. Sayd, V. Silivanov and H. Su, "Design and control of a high-torque and highly backdrivable hybrid soft exoskeleton for knee injury prevention during squatting," *IEEE Robot Autom Lett* **4**(4), 4579–4586 (2019).
- [23] M. K. Shepherd and E. J. Rouse, "Design and validation of a torque-controllable knee exoskeleton for sit-to-stand assistance," *IEEE/ASME Trans Mechatron* **22**(4), 1695–1704 (2017).
- [24] N. Karavas, A. Ajoudani, N. Tsagarakis, J. Saglia, A. Bicchi and D. Caldwell, "Tele-Impedance Based Stiffness and Motion Augmentation for a Knee Exoskeleton Device," *In: 2013 IEEE international conference on robotics and automation*, Karlsruhe, Germany (IEEE, 2013) pp. 2194–2200.
- [25] R. M. de Andrade, P. H. Fabriz Ulhoa, E. A. Fragoso Dias, A. B. Filho and C. B. S. Vimieiro, "Design and testing a highly backdrivable and kinematic compatible magneto-rheological knee exoskeleton," *J Intell Mat Syst Str* **34**(6), 653–663 (2023).
- [26] H. L. Liew and I. Mizuuchi, "Energy Regeneration System for Quasi-Direct Drive Actuated Knee Exoskeleton," *In: 2023 IEEE/SICE International Symposium on System Integration (SII)*, Atlanta, GA, USA (IEEE, 2023) pp. 1–6.
- [27] Z. Wu, M. Yang, Y. Xia and L. Wang, "Mechanical structural design and actuation technologies of powered knee exoskeletons: A review," *Appl Sci* **13**(2), 1064 (2023).
- [28] S. Luo, G. Androwis, S. Adamovich, H. Su, E. Nunez and X. Zhou, "Reinforcement learning and control of a lower extremity exoskeleton for squat assistance," *Front Robot AI* **8**, 702845 (2021).
- [29] S. Luo, G. Androwis, S. Adamovich, E. Nunez, H. Su and X. Zhou, "Robust walking control of a lower limb rehabilitation exoskeleton coupled with a musculoskeletal model via deep reinforcement learning," *J Neuroeng Rehabil* **20**(1), 1–19 (2023).
- [30] X. Gao, J. Si, Y. Wen, M. Li and H. Huang, "Reinforcement learning control of robotic knee with human-in-the-loop by flexible policy iteration," *IEEE Trans Neur Net Learn Syst* **33**(10), 5873–5887 (2021).
- [31] R. Huang, Z. Peng, H. Cheng, J. Hu, J. Qiu, C. Zou and Q. Chen, "Learning-Based Walking Assistance Control Strategy for a Lower Limb Exoskeleton with Hemiplegia Patients," *In: 2018 IEEE/RSJ International Conference on Intelligent Robots and Systems (IROS)*, Madrid, Spain (IEEE, 2018) pp. 2280–2285.
- [32] C. Liu, M. L. Audu, R. J. Triolo and R. D. Quinn, "Neural networks trained via reinforcement learning stabilize walking of a three-dimensional biped model with exoskeleton applications," *Front Robot AI* **8**, 710999 (2021).
- [33] W.-Z. Li, G.-Z. Cao and A.-B. Zhu, "Review on control strategies for lower limb rehabilitation exoskeletons," *IEEE Access* **9**, 123040–123060 (2021).
- [34] G. Masengo, X. Zhang, R. Dong, A. B. Alhassan, K. Hamza and E. Mudoheranwa, "Lower limb exoskeleton robot and its cooperative control: A review, trends, and challenges for future research," *Front Neurorobot* **16**, 913748 (2023).
- [35] S. Luo, G. Androwis, S. Adamovich, E. Nunez, H. Su and X. Zhou, "Robust walking control of a lower limb rehabilitation exoskeleton coupled with a musculoskeletal model via deep reinforcement learning," *J Neuroeng Rehabil* **20**(1), 34 (2023).
- [36] P. E. Gill, W. Murray and M. A. Saunders, "SNOPT: An SQP algorithm for large-scale constrained optimization," *Siam Rev* **47**(1), 99–131 (2005).
- [37] R. Zaman, A. Arefeen, J. Quarnstrom, S. Barman, J. Yang and Y. Xiang, "Optimization-based biomechanical lifting models for manual material handling: A comprehensive review," *Proc Inst Mech Eng Part H: J Eng Med* **236**(9), 1273–1287 (2022).
- [38] J. Denavit and R. S. Hartenberg, "A kinematic notation for lower-pair mechanisms based on matrices," *J Appl Mech* **22**(2), 215–221 (1955).
- [39] Y. Xiang and A. Arefeen, "Two-dimensional team lifting prediction with floating-base box dynamics and grasping force coupling," *Multibody Syst Dyn* **50**(2), 211–231 (2020).
- [40] Y. Xiang, J. S. Arora, S. Rahmatalla and K. Abdel-Malek, "Optimization-based dynamic human walking prediction: One step formulation," *Int J Numer Meth Eng* **79**(6), 667–695 (2009).
- [41] Y. Xiang, J. S. Arora, S. Rahmatalla, T. Marler, R. Bhatt and K. Abdel-Malek, "Human lifting simulation using a multi-objective optimization approach," *Multibody Syst Dyn* **23**(4), 431–451 (2010).

- [42] A. Arefeen and Y. Xiang, “Two-Dimensional Team Lifting Prediction with Different Box Weights,” *In: Proceedings of the ASME. 2020 International Design Engineering Technical Conferences and Computers and Information in Engineering Conference, Online*, (ASME, 2020) pp. V009T09A004. August 17-19, 2020
- [43] Y. Xiang, J. Cruz, R. Zaman and J. Yang, “Multi-objective optimization for two-dimensional maximum weight lifting prediction considering dynamic strength,” *Eng Optimiz* **53**(2), 206–220 (2021).
- [44] M. Bataineh, T. Marler, K. Abdel-Malek and J. Arora, “Neural network for dynamic human motion prediction,” *Expert Syst Appl* **48**, 26–34 (2016).
- [45] H. Zhao and S. Guo, “Annual energy consumption forecasting based on PSOCA-GRNN model,” *Abst Appl Anal* **2014**, 217630 (2014).
- [46] N. A. Hamzaid, R. M. Smith and G. M. Davis, “Isokinetic cycling and elliptical stepping: A kinematic and muscle activation analysis,” *Clin Res Foot Ankle* **1**, 117 (2013).
- [47] A. Wagner, B. Forister and Z. Huot, “EMG analysis of latissimus dorsi, middle trapezius, and erector spinae muscle activity during spinal rotation: A pilot study,” *Physical Therapy Scholarly Projects*, 662 (2019).
- [48] H.-J. Chung, J. S. Arora, K. Abdel-Malek and Y. Xiang, “Dynamic optimization of human running with analytical gradients,” *J Comput Nonlinear Dyn* **10**(2), 021006 (2015).
- [49] R. Zaman, Y. Xiang, R. Rakshit and J. Yang, “Hybrid predictive model for lifting by integrating skeletal motion prediction with an openSim musculoskeletal model,” *IEEE Trans Biomed Eng* **69**(3), 1111–1122 (2022).
- [50] M. Hariri, Y. Xiang, H. J. Chung, R. Bhatt, J. S. Arora and K. Abdel-Malek, “Simulation and Prediction of the Motion of a Human in a Vertical Jumping Task,” *In: 2013 ASME Dynamic Systems and Control Conference*, Munger Center, Palo Alto, CA (Stanford University, 2013).
- [51] S. Zheng, Q. Li and T. Liu, “Multi-phase optimisation model predicts manual lifting motions with less reliance on experiment-based posture data,” *Ergonomics* **66**(9), 1398–1413 (2023).
- [52] M. Sreenivasa, M. Millard, I. Kingma, J. H. van Dieen and K. Mombaur, “Predicting the influence of hip and lumbar flexibility on lifting motions using optimal control,” *J Biomech* **78**, 118–125 (2018).
- [53] J. Zhang, P. Fiers, K. A. Witte, R. W. Jackson, K. L. Poggensee, C. G. Atkeson and S. H. Collins, “Human-in-the-loop optimization of exoskeleton assistance during walking,” *Science* **356**(6344), 1280–1284 (2017).
- [54] Y. Ding, M. Kim, S. Kuindersma and C. J. Walsh, “Human-in-the-loop optimization of hip assistance with a soft exosuit during walking,” *Sci Robot* **3**(15), eaar5438 (2018).
- [55] H. S. Lo and S. Xie, “Optimization and analysis of a redundant 4R spherical wrist mechanism for a shoulder exoskeleton,” *Robotica* **32**(8), 1191–1211 (2014).
- [56] B. Chen, J. Tan, C. Shi and B. Zi, “Development of knee exoskeleton for capturing energy from human knee motion,” *Robotica* **41**(10), 3195–3210 (2023).

## Appendix: Kinematics and dynamics

This research investigates the human model’s kinematics and dynamics through recursive kinematics and Lagrangian dynamics [38, 39]. The equation representing the human dynamics is given as [38, 39]:

$$\tau_{h_i} = \text{tr} \left( \frac{\partial \mathbf{A}_i}{\partial q_i} \mathbf{D}_i \right) - \mathbf{g}^T \frac{\partial \mathbf{A}_i}{\partial q_i} \mathbf{E}_i - \mathbf{f}_k^T \frac{\partial \mathbf{A}_i}{\partial q_i} \mathbf{F}_i - \mathbf{G}_i^T \mathbf{A}_{i-1} \mathbf{z}_0 \quad (1)$$

where the human torque at  $i^{\text{th}}$  joint is represented by  $\tau_{h_i}$ . Equation (1) consists of four components on the right-hand side: inertia and Coriolis torque, the torque caused by gravity, the torque generated by external forces, and the torque arising from external moments:

$$\mathbf{D}_i = \mathbf{I}_i \mathbf{C}_i^T + \mathbf{T}_{i+1} \mathbf{D}_{i+1} \quad (2)$$

$$\mathbf{E}_i = m_i \mathbf{r}_i + \mathbf{T}_{i+1} \mathbf{E}_{i+1} \quad (3)$$

$$\mathbf{F}_i = \mathbf{r}_k \delta_{ik} + \mathbf{T}_{i+1} \mathbf{F}_{i+1} \quad (4)$$

$$\mathbf{G}_i = \mathbf{h}_k \delta_{ik} + \mathbf{G}_{i+1} \quad (5)$$

where the trace of a matrix is denoted as  $\text{tr}(\cdot)$ , and  $\mathbf{A}_i$ ,  $\mathbf{C}_i$  represent global position and acceleration transformation matrices, respectively.  $\mathbf{I}_i$  stands for the inertia matrix of  $i$ ,  $\mathbf{D}_i$  is the recursive inertia and Coriolis matrix,  $\mathbf{E}_i$  is the recursive vector used for gravity torque calculation,  $\mathbf{F}_i$  is the recursive vector for external force-torque calculation, and  $\mathbf{G}_i$  is the recursive vector for external moment torque calculation. The gravity vector is represented as  $\mathbf{g}$ ,  $m_i$  is the mass of link  $i$ , and  $\mathbf{r}_i$  indicates the center

of mass (COM) of link  $i$  in its local frame. For link  $k$ , the external force applied to it is given by the vector,  $\mathbf{f}_k = [0 \ f_{ky} \ f_{kz} \ 0]^T$ . The position of the external force in the  $k^{th}$  local frame is specified by  $\mathbf{r}_k$ . Similarly, for link  $k$ , the external moment applied to it is represented by the vector  $\mathbf{h}_k = [h_x \ 0 \ 0 \ 0]^T$ . The vectors  $\mathbf{z}_0 = [0 \ 0 \ 1 \ 0]^T$  and  $\mathbf{z}_0 = [0 \ 0 \ 0 \ 0]^T$  are used respectively for revolute and prismatic joints. The Kronecker delta is denoted as  $\delta_{ik}$ , and the initial conditions are set as  $\mathbf{D}_{n+1} = [\mathbf{0}]$  and  $\mathbf{E}_{n+1} = \mathbf{F}_{n+1} = \mathbf{G}_{n+1} = [\mathbf{0}]$ . The sensitivities to state variables are thoroughly explained in references [38, 39].

### A.1. Knee exoskeleton dynamics

This study involves the modeling of the electromechanical dynamics of DC motors used in exoskeletons. The equations governing these dynamics are represented as follows [10]:

$$L \frac{dI}{dt} = V - K \frac{d\theta}{dt} - RI \quad (6)$$

$$T_{motor} = KI \quad (7)$$

$$T_l = T_{motor} - J_m \frac{d^2\theta}{dt^2} - b \frac{d\theta}{dt} \quad (8)$$

where  $V$ ,  $I$ ,  $L$ , and  $R$  denote the voltage input, current, inductance, and resistance, respectively. The mechanical parameters  $J_m$ ,  $b$ ,  $K$ , and  $\theta$  represent the rotor moment of inertia, coefficient of viscous friction of the motor, motor torque constant, and rotor angle.  $T_l$  represents the exoskeleton's load torque, and  $T_{motor}$  stands for the motor's output torque. In order for the device to provide the required amount of torque, the gearbox ratios ( $GB_r$ ) are carefully selected. In this context, the exoskeleton comprises both the motor and the gearbox. Hence, the expression for the exoskeleton's output torque ( $\tau_e$ ) is as follows:

$$\tau_e = GB_r \times T_l \quad (9)$$

Moreover, we presume that the exoskeleton's movement corresponds to the motion of human joints. Consequently, the differentiation of the rotor angle  $\dot{\theta}$  and  $\ddot{\theta}$  can be represented using the derivative of the human joint angle  $\dot{q}$  and  $\ddot{q}$  with the corresponding gear ratio:

$$\dot{\theta} = GB_r \times \dot{q} \quad (10)$$

$$\ddot{\theta} = GB_r \times \ddot{q} \quad (11)$$

where  $\dot{q}$  and  $\ddot{q}$  represent the joint's respective angular velocity and acceleration.

### A.2. The human–exoskeleton coupled EOM

The complete dynamics are depicted in the following way [10]:

$$\tau_{h_i} + \tau_{e_i} = \text{tr} \left( \frac{\partial \mathbf{A}_i}{\partial q_i} \mathbf{D}_i \right) - \mathbf{g}^T \frac{\partial \mathbf{A}_i}{\partial q_i} \mathbf{E}_i - \mathbf{f}_k^T \frac{\partial \mathbf{A}_i}{\partial q_i} \mathbf{F}_i - \mathbf{G}_i^T \mathbf{A}_{i-1} \mathbf{z}_0 \quad (12)$$

where  $\tau_{e_i}$  represents the exoskeleton's output torque for the  $i^{th}$  joint. A two-stage active-and-passive algorithm in references [38, 39] is utilized to compute the GRFs.